

Hadley Cell Dynamics in a Primitive Equation Model. Part I: Axisymmetric Flow

HYUN-KYUNG KIM AND SUKYOUNG LEE

Department of Meteorology, The Pennsylvania State University, University Park, Pennsylvania

(Manuscript received 24 January 2000, in final form 8 February 2001)

ABSTRACT

A strategy is adopted that applies the mean meridional circulation (MMC) equation to *two* different steady states of a primitive equation model. This allows for the investigation of the mechanisms behind the sensitivity of the Hadley cell structure to individual source terms in an axisymmetric circulation. Specifically, the strategy allows the MMC response to the individual source terms to be partitioned into direct and indirect components.

The model's Hadley cell strengthens and broadens as the viscosity of the model is increased. It is found that a substantial portion of this sensitivity is attributable to diabatic heating and surface friction changes, which are ultimately induced by changes in viscosity. Similar behavior is found as the meridional gradient of the radiative-convective equilibrium temperature is increased, except that in this case the indirect response arises through the viscosity and surface friction change. In both cases, the changes in the static stability change are found to be of secondary importance.

It is found that the latitudinal extent of the Hadley cell is more sensitive to the meridional temperature gradient than to the static stability. However, when the static stability is decreased (increased) by a sufficient amount, the Hadley cell becomes narrower (broader). Additional analyses indicate that the change in Hadley cell width is a response to the change in Hadley cell strength.

1. Introduction

The question of how much of the Hadley cell is attributable to individual heat and momentum sources is a long-standing problem. Of particular interest is the role of the midlatitude baroclinic eddy heat and momentum fluxes in driving the Hadley cell. In fact, as will be further motivated in Part II (Kim and Lee 2001, hereafter KL), the primary goal of this two-part study is to better understand 1) how important the eddy fluxes are in driving the Hadley cells, 2) through what physical processes the impact of eddy fluxes are manifested, and 3) how sensitive these results are to an imposed diabatic heating field.

While a linear diagnostic equation [Eliassen 1951; Kuo 1956; the mean meridional circulation (MMC) equation hereafter] may be used for this purpose, its use implicitly assumes that each momentum and heat source in the equation is independent from each other. However, for atmospheric motion with a sufficiently long timescale, this independence assumption becomes highly questionable. Taking the Ferrel cell as an example, Chang (1996) finds that surface friction can be treated as being independent of eddy fluxes only for times shorter than the radiative relaxation timescale.

In order to overcome the above problem, we adopt a strategy (see section 2, and also KL), whereby the MMC diagnostic equation is applied to *two* different steady states, which are obtained from a primitive equation (PE) model. This strategy exploits the fact that in the model experiments, the *ultimate* cause, that leads to the difference between the *two* steady states, can be precisely specified. For example, as was done by both Becker et al. (1997) and KL, one is able to unambiguously evaluate the effect of the eddy fluxes, by comparing the axisymmetric and nonaxisymmetric model runs.

The result, however, will be meaningful only if the axisymmetric flow is faithfully calculated and properly understood. However, judging the validity of the axisymmetric flow is troublesome, as an axisymmetric flow is never realized in the atmosphere. One may circumvent this difficulty by benchmarking the behavior of the axisymmetric flow against that described by Held and Hou (1980, hereafter HH), as the Hadley cell found in their study is well understood, and provides a theoretical foundation for axisymmetric circulations. In fact, this is the approach that we adopt. Accordingly, the main goal of this paper is to set the stage for KL, by analyzing the axisymmetric model's Hadley cell structure, and benchmarking the result against that of HH. However, the scope of this paper is by no means limited to this benchmarking. By applying the strategy of combining the MMC diagnostic equation for two different axisymmetric runs, we reveal subtleties behind the Hadley cell sensitivity to important model parameters.

Corresponding author address: Dr. Sukyoung Lee, Dept. of Meteorology, The Pennsylvania State University, University Park, PA 16802.
E-mail: sl@essc.psu.edu

The paper is organized as follows. Section 2 outlines the strategy of our numerical experiments and diagnoses. The PE model and a diagnostic equation are described in section 3. Sections 4 and 5 present the results. The discussion and concluding remarks follow in section 6.

2. Strategy

As stated above, our strategy is to apply the MMC equation diagnostics to two different steady states from the axisymmetric version of the PE model. Denoting the meridional mass streamfunction calculated directly from the PE model run as Ψ , it is convenient to introduce a symbolic equation for the quasigeostrophic (QG) MMC:

$$\Psi_D = L^{-1}(S_1 + S_2 + S_3 \dots + S_n), \quad (1)$$

where Ψ_D is the quasigeostrophic diagnosed mass streamfunction, L the linear operator defined by (4) below, and $S_i (i = 1, \dots, n)$ the individual heat and momentum source terms. Equation (1) expresses an estimate of the MMC in terms of the sum of the individual source terms. Suppose that two steady states are obtained by perturbing one of the source terms, say S_1 , and that the MMC equation is *perfect*, that is, $\Psi_D = \Psi$. Denoting the change in S_1 as δS_1 and the change in the MMC as $\delta \Psi$, if the other source terms are not influenced by δS_1 , then the MMC response to δS_1 must be $\delta \Psi = L^{-1} \delta S_1$. However, the circulation change due to δS_1 can change the other source terms, and this in turn can further alter the MMC. In this situation, the MMC response to the changes in the other source terms must be taken into account to fully explain $\delta \Psi$.

The equation for the “perturbation” MMC,

$$\delta \Psi_D = L^{-1}(\delta S_1 + \delta S_2 + \delta S_3 \dots + \delta S_n), \quad (2)$$

is a useful tool in distinguishing between “direct” and “indirect” responses to the externally imposed δS_1 . Mathematically, the direct and indirect contributions are defined as $L^{-1} \delta S_1$ and $(L^{-1} \sum_{n=2}^N \delta S_n)$, respectively. Note that we continue to assume that S_1 is the only source term explicitly perturbed.

This subtlety behind the concept of direct and indirect responses may be illustrated by considering two model steady states where one run is perturbed relative to the other by changing the value of the diffusion coefficient K_v in (6). In that case, $\delta S_1 = \delta D^U$, and thus the above definition regards $L^{-1} \delta D^U$ as the direct response. However, δD^U is nonzero not only due to the change in K_v , but also because of changes in $\partial u / \partial p$ [see (6)]. Because the latter changes in δD^U can arise from nonlinear processes that involve the other source terms, $L^{-1} \delta D^U$ includes not only a direct response to the change in K_v , but also indirect responses through changes in $\partial u / \partial p$, induced in part by the other source terms. Nevertheless, we elect to use the term “direct” for $L^{-1} \delta D^U$, as the parameter being varied, K_v , is part of D^U .

3. Model description and methodology

a. The primitive equation model

The PE model used in this study is based on the dynamical core of the Geophysical Fluid Dynamics Laboratory (GFDL) general circulation model (e.g., see Feldstein 1994), which was originally provided by Isaac Held of GFDL. In this study, we use a zonally symmetric version of this model. The horizontal scale is truncated at rhomboidal 30, and there are 20 equally spaced sigma levels.

Following the formulation of HH, the model is forced by relaxing the potential temperature toward a “radiative–convective equilibrium” profile, Θ_E . Within the model’s troposphere, Θ_E takes the form of

$$\frac{\Theta_E(\theta, \sigma)}{\Theta_0} = 1 - \frac{1}{3} \Delta_h (3 \sin^2 \theta - 1) - \Delta_v \left(\frac{h}{H_s} \ln \sigma + \frac{1}{2} \right),$$

where θ is latitude; Θ_0 the global mean values of Θ_E ; Δ_h and Δ_v the fractional change in Θ_E from equator to Pole, and from the tropopause to surface, respectively; and h and H_s are the scale height, and the tropopause height, respectively. Instead of imposing a rigid upper boundary as in HH, this model’s tropopause is defined by reversing the meridional gradient of Θ_E at that level. Also, in order to keep the problem as simple as possible, the meridional structure of Θ_E is held symmetric about the equator for all experiments.

The models viscosity and conductivity take the form of $(g^2 K_v / p_s^2) (\partial / \partial \sigma) (\rho^2 (\partial \mathbf{u} / \partial \sigma))$ and $(g^2 K_c / p_s^2) (\partial / \partial \sigma) (\rho^2 (\partial \Theta / \partial \sigma))$, respectively, where $\mathbf{u} = (u, v, 0)$, ρ is the density, and p_s is the surface pressure. In accord with HH, the vertical diffusion coefficient K_v is chosen so that the dynamic diffusion coefficient ρK_v is constant with height within the troposphere. Since ρ decreases with height, for brevity, throughout this paper the surface value of K_v , denoted as K_{v0} , is provided. Above the tropopause, in order to ensure computational stability, the value of K_v is set to $1 \text{ m}^2 \text{ s}^{-1}$. The surface ($\sigma = 1$) momentum fluxes are given by $-(\rho g / p_s) K_v (\partial \mathbf{u} / \partial \sigma) = C \mathbf{u}$, where C is a constant linear drag coefficient. At the uppermost level of the model, the momentum flux is set to zero. Again, following HH, the sensible heat flux is set to zero at both the upper and lower boundaries. Although not shown, we found the effect of the surface heat flux to be very small and mostly confined to within a shallow layer adjacent to the lower boundary. Except for a few limited runs, we also set the Prandtl number, K_v / K_c , equal to 1.

For all experiments, the model parameters are fixed as: $h = 8.0 \times 10^3 \text{ m}$, $H_s = 1.0 \times 10^4 \text{ m}$, $\Theta_0 = 300 \text{ K}$, $C = 0.01 \text{ m s}^{-1}$. The values of $\Theta_0 \Delta_h$ and $\Theta_0 \Delta_v$ are varied over the range 40, 60, 80 K, and 5, 8.3, 12.5, 16.7, 25 K, respectively. Given these ranges of parameters, when the value of the vertical diffusion coefficient K_{v0} is varied in steps of $0.1 \text{ m}^2 \text{ s}^{-1}$, the smallest value possible for a steady-state solution turns out to be 0.5

$\text{m}^2 \text{s}^{-1}$. Therefore, the parameter values for our control run are chosen as $K_{\nu 0} = 0.5 \text{ m}^2 \text{ s}^{-1}$, $\Delta_h = 60 \text{ K}/\Theta_0$, $\Delta_v = 12.5 \text{ K}/\Theta_0$, and $\tau = 40$ days, where τ is the radiative relaxation timescale.

b. A diagnostic equation for the MMC

Given that our model consists of primitive equations, it would be self-consistent to choose an equation for the MMC, derived from the PE set [e.g., see (4) in Pfeffer (1981)]. However, for ease of obtaining a solution, we invoke the QG approximation. As will be shown later, even within the deep Tropics, the MMC obtained with the QG approximation agrees reasonably well with that found in the nonlinear PE model.

Under the assumptions of zonal symmetry and quigeostrophy, the following MMC equation (see Haynes and Shepherd 1989) is obtained:

$$L\Psi_D = \frac{2\pi a^2}{g} \left[-\frac{2\Omega\mu}{a(1-\mu^2)^{1/2}} \frac{\partial F}{\partial p} + \frac{R}{a^2 p} \frac{\partial Q}{\partial \mu} \right], \quad (3)$$

where p is pressure, $\mu = \sin\theta$, R the gas constant, and L is a linear operator. On the right-hand side of (3), F and Q represent momentum and thermal sources, respectively. The linear operator, L , takes the form

$$L = \frac{R\Gamma}{a^2 p} \frac{\partial^2}{\partial \mu^2} + \frac{4\Omega^2 \mu^2}{(1-\mu^2)} \frac{\partial^2}{\partial p^2}, \quad (4)$$

where $\Gamma = -\overline{T}(\partial \ln \overline{\Theta} / \partial p)$ is the static stability parameter and $\overline{T}(p)$ and $\overline{\Theta}(p)$ are the horizontally averaged temperature and potential temperature, respectively. In order to describe the results from such calculations, it is convenient to rewrite (3) as

$$L\Psi_D = F^M + D^U + SF + F^H + H + D^T, \quad (5)$$

where the source terms on the rhs of (5) take the form

$$\begin{aligned} F^M &= \frac{4\pi\mu}{g(1-\mu^2)} \frac{\partial}{\partial p} \left\{ \frac{\partial}{\partial \mu} [(1-\mu^2)\overline{u'v'}] \right\} \\ F^H &= -\frac{2\pi R}{agp} \frac{\partial}{\partial \mu} \left\{ \frac{\partial}{\partial \mu} [(1-\mu^2)^{1/2}\overline{v'T'}] \right\} \\ D^U &= -\frac{4\pi a\mu}{(1-\mu^2)^{1/2}} \frac{\partial}{\partial p} \left\{ \frac{\partial}{\partial p} \left[\rho^2 g K_v \frac{\partial u}{\partial p} \right] \right\} \\ D^T &= \frac{2\pi R}{p} \frac{\partial}{\partial \mu} \left\{ \frac{\partial}{\partial p} \left[\rho^2 g K_v \frac{\partial \Theta}{\partial p} \right] \right\} \\ SF &= \frac{4\pi a\mu}{(1-\mu^2)^{1/2}} \left[\frac{\rho C u(p_0)}{(\Delta p)^2} \right] \\ H &= \frac{2\pi R}{gp} \frac{\partial}{\partial \mu} \left(\frac{T_E - T}{\tau} \right). \end{aligned} \quad (6)$$

The terms F^M and F^H represent eddy momentum and heat sources, respectively. The two mixing terms, D^U

and D^T , correspond to the diffusion terms in the zonal momentum and thermodynamic equations, respectively. The former represents viscosity, and the latter conductivity. The momentum source due to surface friction is represented by SF; in (6), $\Delta p = p_s \Delta \sigma_{kx}$, where $\Delta \sigma_{kx}$ represents the thickness of the lowest two half-sigma levels. In calculating D^U , the value of $\partial u / \partial p$ at the surface is set to zero, as this is separately evaluated in SF. The heat source due to the meridional convergence of the diabatic heating is represented by H , where T_E is the temperature corresponding to Θ_E defined earlier.

In practice, instead of solving directly for Ψ_D from (3), the ω equation is solved and then Ψ_D is calculated from ω using the continuity equation. This is because it is more convenient to apply boundary conditions on ω than on Ψ_D . Following Plumb (1982) and Haynes and Shepherd (1989), the latitudinal structure of each variable in the ω equation is expressed in terms of either Hough functions, $\Theta_n(\mu)$, or associated functions, $B_n(\mu)$ (Longuet-Higgins 1968):

$$\begin{aligned} \omega(p, \mu) &= \sum_n \omega_n(p) \Theta_n(\mu) \\ v(p, \mu) &= \sum_n v_n(p) B_n(\mu) \\ Q(p, \mu) &= \sum_n Q_n(p) \Theta_n(\mu) \\ F(p, \mu) &= \sum_n F_n(p) \mu B_n(\mu), \end{aligned} \quad (7)$$

where the $\Theta_n(\mu)$ satisfy the following eigenvalue equation

$$\frac{d}{d\mu} \left[\frac{(1-\mu^2) d\Theta_n}{\mu^2 d\mu} \right] - \epsilon_n \Theta_n = 0, \quad (8)$$

and the $B_n(\mu)$ are related to the $\Theta_n(\mu)$ by

$$\Theta_n(\mu) = \frac{d}{d\mu} [B_n(\mu)(1-\mu^2)^{1/2}]. \quad (9)$$

As described in Plumb (1982), because of convenience in applying boundary conditions, that is, no meridional flow at the Poles, we solve for $B_n(\mu)$ using (A1). Via (9), $\Theta_n(\mu)$ is then calculated from $B_n(\mu)$. It is important to note that both $B_n(\mu)$ and $\Theta_n(\mu)$ must be orthogonal functions [see (A3) and (A4)]. However, because $\Theta_n(\mu)$ is obtained through (9), inaccuracies introduced in estimating the meridional finite differencing can undermine the required orthogonality for higher-order modes whose meridional scales are relatively small. We found that this inaccuracy, which appears to be rather insignificant as shown in Fig. A1a, can greatly distort both the sources and responses, in particular at low latitudes. Because such inaccuracies can be erroneously attributed to the breakdown of the QG approximation near the equator, rather than the violation of orthogonality, in the appendix we describe an example of the expansion and a simple remedy for improving the accuracy.

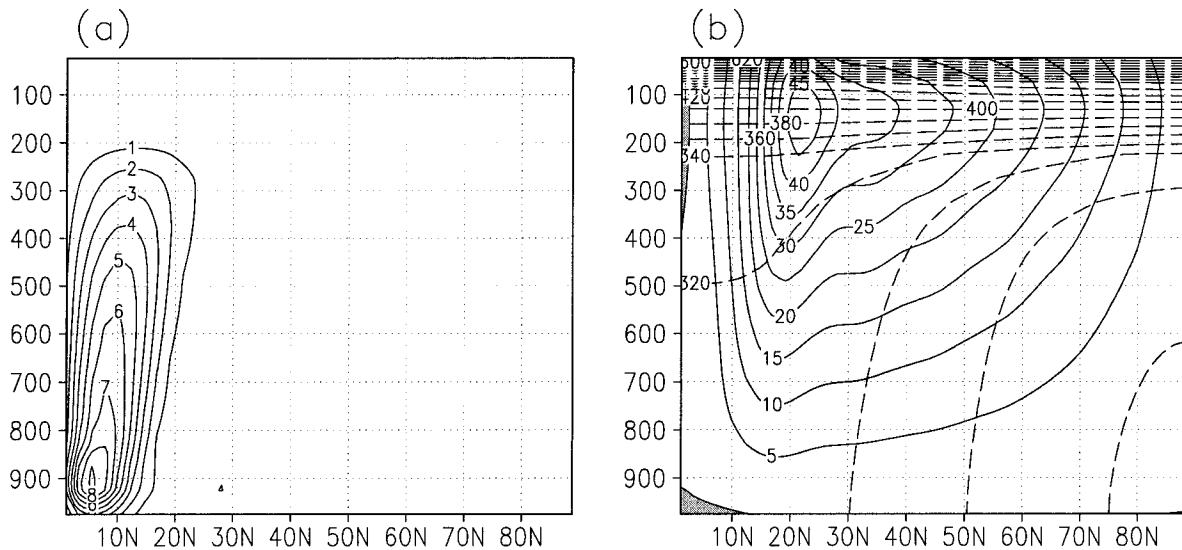


FIG. 1. Axisymmetric (a) mass streamfunction, (b) zonal wind (solid line) and potential temperature (dashed line) in the control case. Contour interval in (a) is $1 \times 10^9 \text{ kg s}^{-1}$ and in (b) 5 m s^{-1} and 20 K . Zero contours for (a) are omitted and the shaded area in (b) indicates the region of easterlies.

By substituting (7) into the ω equation (e.g., see Haynes and Shephard 1989), one obtains an ordinary differential equation for the expansion coefficients, ω_n ,

$$\frac{4\Omega^2 a^2 p}{R} \frac{d^2 \omega_n}{dp^2} + \Gamma \epsilon_n \omega_n = \frac{2\Omega a p}{R} \frac{dF_n}{dp} - \epsilon_n Q_n. \quad (10)$$

The solution to (10) is then obtained by imposing boundary conditions that no flow is allowed across the top and bottom of the model atmosphere. Accordingly, the lower boundary of the model satisfies $D\Phi/Dt = 0$ rather than $\omega = 0$. The implications of using the in-

accurate latter boundary condition is discussed by Haynes and Shepherd (1989).

4. The control case

A steady state solution of the axisymmetric circulation for the control run is obtained using the zonally symmetric version of the model. The mass streamfunction, Ψ , is shown in Fig. 1a, and the corresponding zonal wind and potential temperature fields are displayed in Fig. 1b. Because the model is symmetric about the equator, throughout this paper, results from only one hemisphere are presented. Consistent with the HH theory, a strong and sharp subtropical jet is located close to the poleward boundary of the Hadley cell. Therefore, for the axisymmetric flow, we define the latitude of the subtropical jet maximum as the poleward end of the Hadley cell.

As motivated in section 2, we use the MMC equation to investigate rather subtle mechanisms behind the Hadley cell sensitivity to a few selected model parameters. Before presenting the results of the sensitivity investigation, we first compare the diagnosed mass streamfunction, Ψ_D , obtained from the MMC equation, against that of the PE model. Figure 2 shows the total diagnosed Ψ_D response to all source terms, D^u , SF, H , and D^T [see (6) for the expressions], for the control case. The overall structure of the diagnosed Hadley cell resembles that of the PE model (Fig. 1a), although the intensity of the former is about 15% weaker than that of the latter. Given that the QG approximation is invoked, such an agreement seems rather impressive.

5. Sensitivity and mechanisms

In this section, we examine the sensitivity of the axisymmetric circulation to (i) the viscosity and conduc-

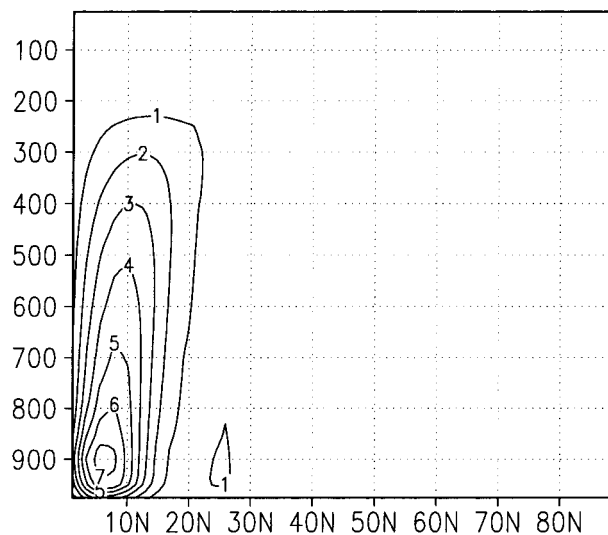


FIG. 2. The QG diagnostic mass streamfunction response to total forcing and damping. Contour interval is $1 \times 10^9 \text{ kg s}^{-1}$. Zero contours are omitted.

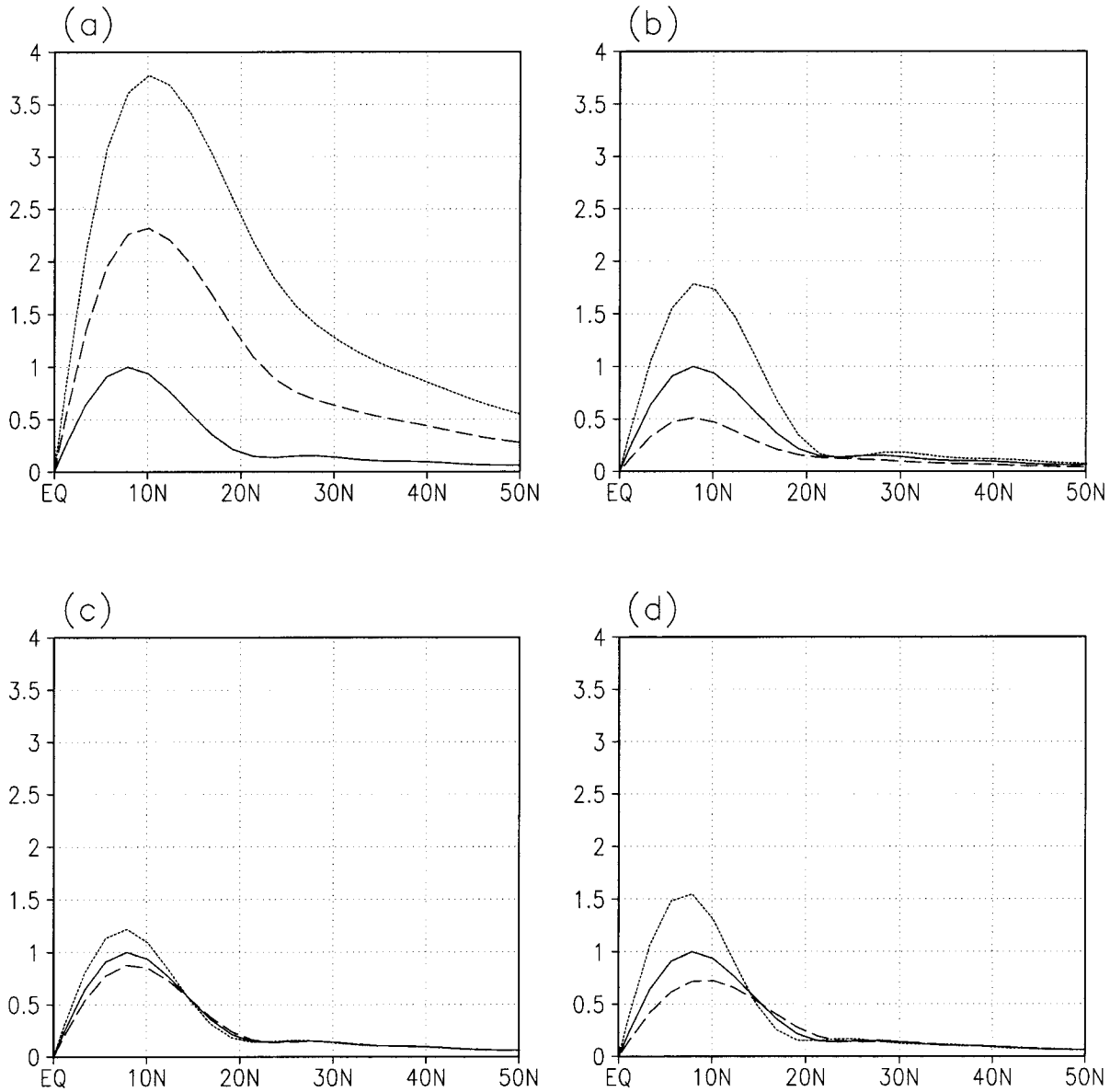


FIG. 3. Vertically integrated axisymmetric mass streamfunctions normalized by the maximum value of the control case. (a) Dotted line for $K_{v0} = 5.0 \text{ m}^2 \text{ s}^{-1}$, dashed line for $2.5 \text{ m}^2 \text{ s}^{-1}$, and solid line for $0.5 \text{ m}^2 \text{ s}^{-1}$; (b) dotted line for $\Theta_0 \Delta_h = 80 \text{ K}$, solid line for 60 K , and dashed line for 40 K ; (c) dotted line for $\Theta_0 \Delta_v = 8.33 \text{ K}$, solid line for 12.5 K , and dashed line for 16.67 K ; and (d) dotted line for $\Theta_0 \Delta_v = 5 \text{ K}$, solid line for $\Theta_0 \Delta_v = 12.5 \text{ K}$, and dashed line for $\Theta_0 \Delta_v = 25 \text{ K}$. Solid lines represent the control case.

tivity, to (ii) the meridional gradient of the equilibrium temperature field, Δ_h , which changes the diabatic heating source H , and to (iii) the vertical gradient of the equilibrium temperature field, Δ_v , which measures the static stability of the model atmosphere. Note that (i) and (ii) involve changes to the source terms, whereas (iii) involves changes in the static stability that alters only the linear operator defined by (4), not H [see (6)]. For these calculations, we will be examining the sensitivity of both the width and strength of Hadley cell to

changes in the source terms and the static stability, however, with the main focus toward the Hadley cell width.

At least in the inviscid limit, the width of the Hadley cell given by HH is proportional to the square root of the meridional gradient of the equilibrium temperature field; however, it is independent of the static stability. On the other hand, the analytic solution of Schneider (1977) predicts that the Hadley cell width is proportional to the static stability. As pointed out by HH, the parametric dependency of the Hadley cell width rests, in

part, on whether thermal wind adjustment is accomplished by changes in $\partial\Theta/\partial y$, $\partial\Theta/\partial z$, or both. We infer the adjustment process by comparing different model runs with different parameter settings. For example, if the Hadley cell width changes as the value of Δ_h is varied, then one may infer that the adjustment process is accomplished, at least in part, by changes in $\partial\Theta/\partial y$.

Because there is no theoretical basis to expect that the Hadley cell's width depends on surface friction, the sensitivity to the value of the drag coefficient, C , is not sought. Having shown that the Ψ_D compares well with its PE counterpart, we perform these following diagnosis.

a. Subgrid-scale mixing: Viscosity and conductivity

While the precise mechanisms that determine the internal viscosity of the atmosphere remain illusive, at least in the tropical troposphere, it seems safe to assume that the atmosphere is moderately viscous (Lindzen and Farrell 1980; HH). Together with the finding that the structure of the MMC in axisymmetric flows is very sensitive to the value of the viscosity coefficient (HH; Becker et al. 1997; Plumb and Eluszkiewicz 1999), this premise begs for an investigation of the sensitivity of the MMC to driving by viscous processes.

Figure 3a shows the vertically integrated Ψ , $\int_0^1 \Psi d\sigma$, for $K_{v0} = 0.5, 2.5,$ and $5.0 \text{ m}^2 \text{ s}^{-1}$, respectively. The value of Ψ is normalized by the maximum value of the control case ($K_{v0} = 0.5 \text{ m}^2 \text{ s}^{-1}$). Consistent with the previous studies referenced above, increasing the value of K_v results in a stronger and wider Hadley cell. Is this sensitivity attributable entirely to the adjustment of the atmosphere to the momentum and temperature mixing [i.e., δD^U and δD^T (5)] or does the change in K_{v0} alter other terms on the rhs of (5) and thus indirectly influence Ψ ?

In order to answer this question, we perform additional calculations whose rationale was outlined in section 2. For the axisymmetric flow, (5) can be rewritten as

$$L\Psi_D = H + SF + D^U + D^T. \quad (11)$$

Separating L , Ψ_D , and source terms [rhs of (11)] into a control value and the deviation from the control value, that is, $L = L_{\text{ctl}} + \delta L$, $\Psi_D = \Psi_{D,\text{ctl}} + \delta\Psi_D$, and substituting these into (11), neglecting the term $\delta L\delta\Psi_D$, and using the relationship $L_{\text{ctl}}\Psi_{D,\text{ctl}} = H_{\text{ctl}} + SF_{\text{ctl}} + D_{\text{ctl}}^U + D_{\text{ctl}}^T$, we obtain

$$\begin{aligned} \delta\Psi_D \approx & L_{\text{ctl}}^{-1}\delta H + L_{\text{ctl}}^{-1}\delta SF + L_{\text{ctl}}^{-1}\delta D^U + L_{\text{ctl}}^{-1}\delta D^T \\ & + L_{\text{ctl}}^{-1}(-\delta L\Psi_{D,\text{ctl}}), \end{aligned} \quad (12)$$

where δ refers to the difference between a more viscous case and the control case. While the first four terms on the rhs of (12) represent the change in the MMC response, $\delta\Psi$, driven by the changes in the individual source terms, the last term on the rhs of (12) accounts for the effect of the static stability change.

Figure 4a shows sum of all terms on the rhs of (12), obtained from the MMC equation. The most viscous case ($K_{v0} = 5.0 \text{ m}^2 \text{ s}^{-1}$) is used for this calculation. Although the amplitude of $\delta\Psi_D$ is about 20% smaller than that of the actual $\delta\Psi$ (not shown) obtained from the PE model, the former captures the structure of the latter reasonably well. The fact that $\delta\Psi_D$ captures the essence of the actual $\delta\Psi$ can be inferred from a comparison of Figs. 4a and 2. Consistent with Fig. 3a, Fig. 4a clearly indicates a strengthening and widening of the Hadley cell, relative to that shown in Fig. 2.

To answer the question raised above, we inspect Figs. 4b–f. It turns out that the direct response to δD^U (Fig. 4d) dominates the total response, however, Figs. 4b and 4c demonstrate that the sensitivity of the Hadley cell to the viscosity amplifies through indirect effects, such as changes in the diabatic heating and surface friction, and their collective effects are not negligible. The change in static stability (Fig. 4f) also enhances the sensitivity, however, its role is relatively minor.

As stated above, the response to the thermal conductivity change is rather small (Fig. 4e), and it is for this reason that the nonzero change in other source terms, such as diabatic heating, are interpreted solely based on the effect of the viscosity, δD^U . Performing identical analyses on outputs from runs with smaller values of K_v , that is, larger Prandtl numbers, yields results that are essentially unchanged. Therefore, we conclude that at least within the parameter space explored here, the thermal conductivity plays a rather minor role.

b. Meridional temperature gradient

Figure 3b shows the sensitivity of the Hadley cell structure to the meridional gradient of the equilibrium temperature field, Δ_h ($\Theta_0\Delta_h = 40, 60,$ and 80 K), for our least viscous case (i.e., $K_{v0} = 0.5 \text{ m}^2 \text{ s}^{-1}$). Recall that the least viscous case with $\Theta_0\Delta_h = 60 \text{ K}$ corresponds to the control case. Consistent with the analytical solution for the inviscid limit given by HH, the width and strength of Hadley cell increase as $\Theta_0\Delta_h$ increases.

Diagnostic analyses based on (12) are also performed, where δ now denotes the difference between the case with the strongest meridional gradient of the equilibrium temperature field ($\Theta_0\Delta_h = 80 \text{ K}$) and the control case. Again, $\delta\Psi_D$ from (12) (Fig. 5a) captures the structure of the actual $\delta\Psi$ from PE models reasonably well although the amplitude of the former is about 38% smaller than the latter. As expected, the change in the diabatic heating (Fig. 5b) explains most of $\delta\Psi$ except near the surface where the change in the surface friction has a more important role in strengthening the Hadley cell (Fig. 5c). As Δ_h increases, the change in the vertical mixing of zonal momentum also strengthens and broadens the Hadley cell (Fig. 5d).

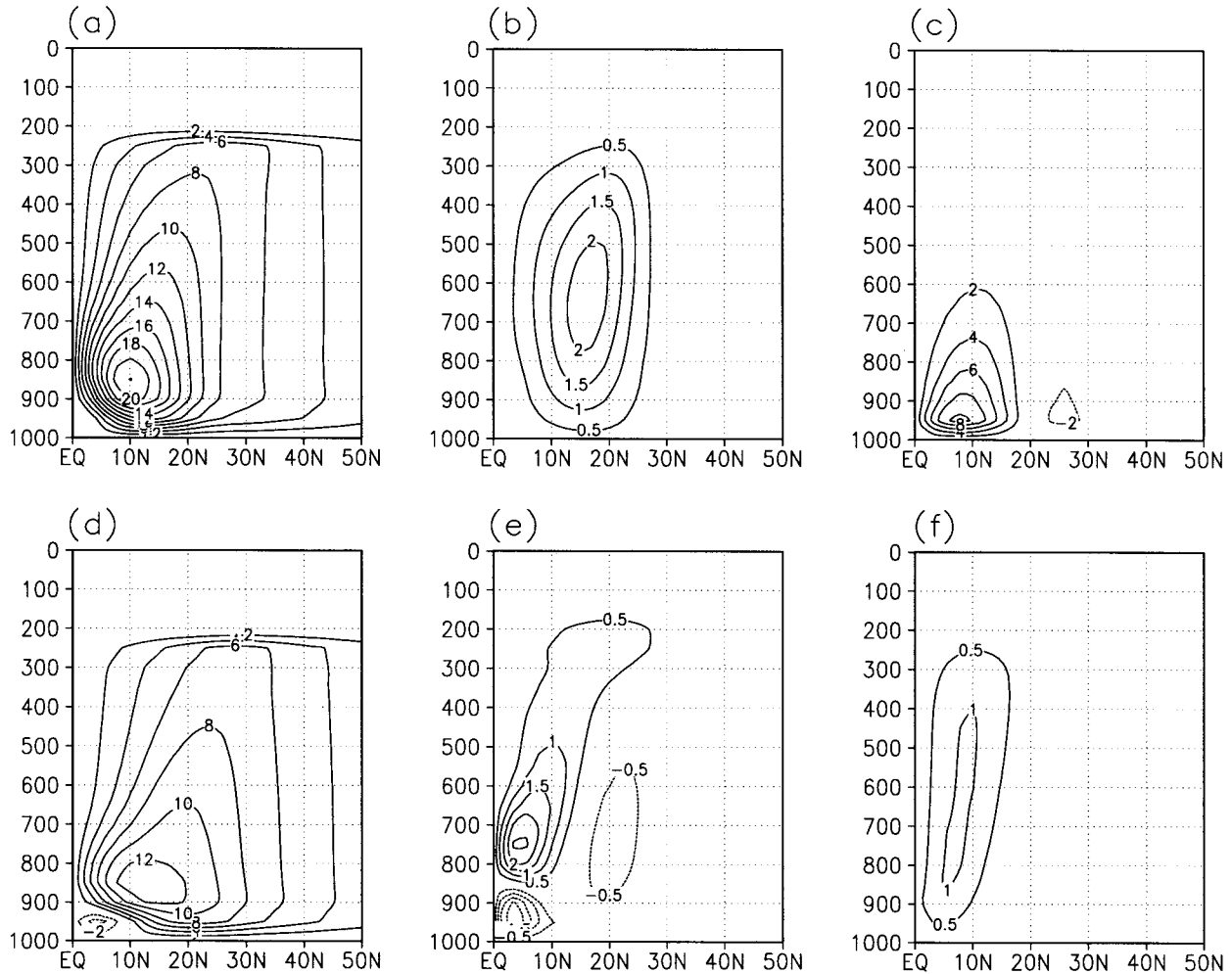


FIG. 4. Differences of QG diagnostic mass streamfunction responses between $K_{v0} = 5.0 \text{ m}^2 \text{ s}^{-1}$ and control case. (a) Approximated total difference, $\delta\Psi$; due to (b) the change in the diabatic heating (δH), (c) the change in the surface friction (δSF), (d) the change in the vertical mixing of zonal momentum (δD^u), (e) the change in the vertical mixing of enthalpy (δD^T), and (f) the change in the static stability (δL). Contour interval is $1 \times 10^9 \text{ kg s}^{-1}$ and zero contours are omitted.

c. Static stability

Fixing the value of K_{v0} at $0.5 \text{ m}^2 \text{ s}^{-1}$, that is, the value used for the control case, when the value of Δ_v is varied by the same fractional amount as Δ_h , that is, $\Theta_0 \Delta_v = 8.33, 12.5,$ and 16.67 K , the width of the Hadley cell exhibits virtually no sensitivity to Δ_v (see Fig. 3c). Given that the Hadley cell width is sensitive to the nature of the temperature adjustment required by thermal wind balance (HH), this result implies that in a relatively inviscid flow the temperature adjustment is realized mostly through the changes in the meridional temperature gradient, rather than changes in the static stability. This result adds confidence to the prediction of the HH theory developed under the Boussinesq approximation.

Although unrealistic, if the static stability is varied by a sufficient amount relative to the control case where $\Theta_0 \Delta_v = 12.5 \text{ K}$, that is, $\Theta_0 \Delta_v = 5$ and 25 K , the Hadley

cell width does exhibit a systematic change. As shown in Fig. 3d, as the static stability increases, the Hadley cell broadens and weakens.

NARROWING OF THE HADLEY CELL

We next investigate how the change in Hadley cell width comes about in response to the static stability change. Because the static stability parameter appears in the coefficient of the linear operator [see (5)], one might expect that the last term on the rhs of (12)¹ accounts for the change of the Hadley cell width. However,

¹ Now δ denotes the difference between the weak static stability ($\Theta_0 \Delta_v = 5 \text{ K}$) and the control case.

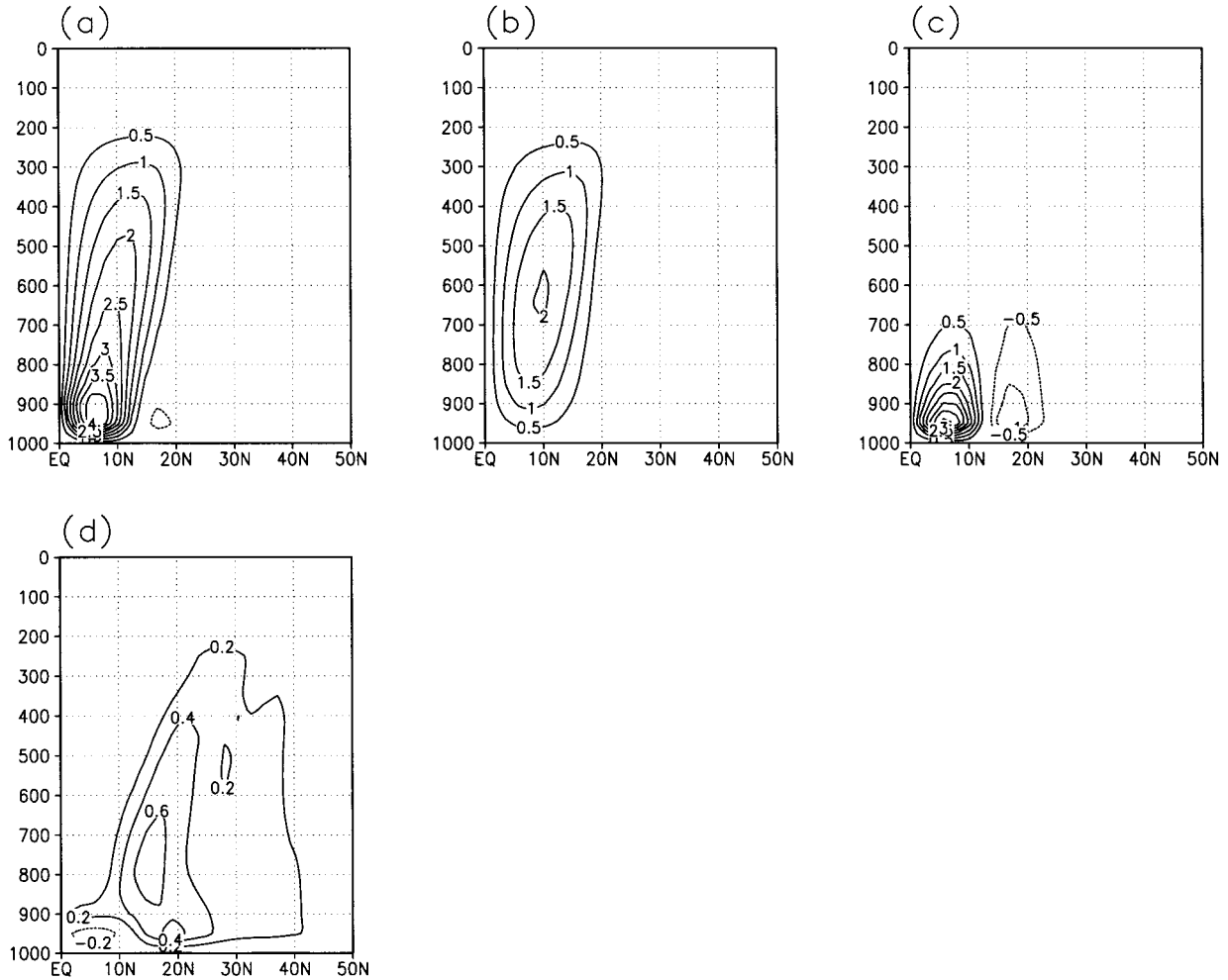


FIG. 5. Differences of QG diagnostic mass streamfunction responses between $\Theta_0\Delta_s = 80$ K and control case. (a) Approximated total difference, $\delta\Psi$; due to (b) the change in the diabatic heating (δH), (c) the change in the surface friction (δSF), and (d) the change in the vertical mixing of zonal momentum (δD^v). Contour interval is 1×10^9 kg s^{-1} and zero contours are omitted.

the diagnosis of (12) for the $\Theta_0\Delta_s = 5$ K case² indicates that the narrowing of the Hadley cell as the static stability decreases is attributable to the change in the diabatic heating (Fig. 6b), rather than changes in the static stability (Fig. 6c). The latter term mainly contributes toward strengthening of the Hadley cell.

In order to better understand the process by which the Hadley cell narrows as the static stability is reduced, we consider the following form of thermodynamic energy equation:

$$-\delta\Gamma \frac{\partial\omega}{\partial y} - \Gamma \frac{\partial\delta\omega}{\partial y} \approx \frac{\partial\delta Q}{\partial y}, \quad (13)$$

² Note that because of the large differences in the static stability between the $\Theta_0\Delta_s = 5$ K case and the control case, the neglect of $\delta L\delta\Psi_D$ results in a rather large discrepancy between the amplitude of $\delta\Psi_D$ (Fig. 6a) and that of the actual $\delta\Psi$. Nevertheless, $\delta\Psi_D$ from (12) captures the structure of the actual $\delta\Psi$ remarkably well, suggesting that (12) remains as a useful diagnostic tool if one is only concerned with the width of the Hadley cell.

where $\omega = \omega_{\text{ctl}} + \delta\omega$, and Γ is assumed to be constant in y . Here, we assume that the adiabatic heating (cooling) balances the diabatic cooling (heating), and that the static stability varies only vertically. The second term on the lhs of (13) represents the MMC response, $\delta\omega$, to the static stability change. Given that the Hadley cell intensifies as the static stability decreases, and that the atmosphere is considered to be statically stable, within the region of the Hadley cell, the second term must be negative and the first term positive. Thus, the process represented by the first (second) term drives an indirect (direct) cell. For reasons to be described below, we separate $\delta\omega$ into $\delta\omega^* + \delta\omega^H$, where $\delta\omega^H$, which is equivalent to $L_{\text{ctl}}^{-1}\delta H$ [see (12)], is the MMC response to δH , where $\delta H \propto \partial(\delta Q)/\partial y$ [see (13)]. Apparently, δH and $\delta\omega^H$ are nonzero because the two terms on the lhs of (13) do not exactly cancel each other. The response of the MMC to all other effects is represented by $\delta\omega^*$.

Figures 7a and 7b show $-\delta\Gamma\omega^*$ and $-\Gamma\delta\omega^*$, respectively, where $\delta\omega^*$ is obtained from the MMC equa-

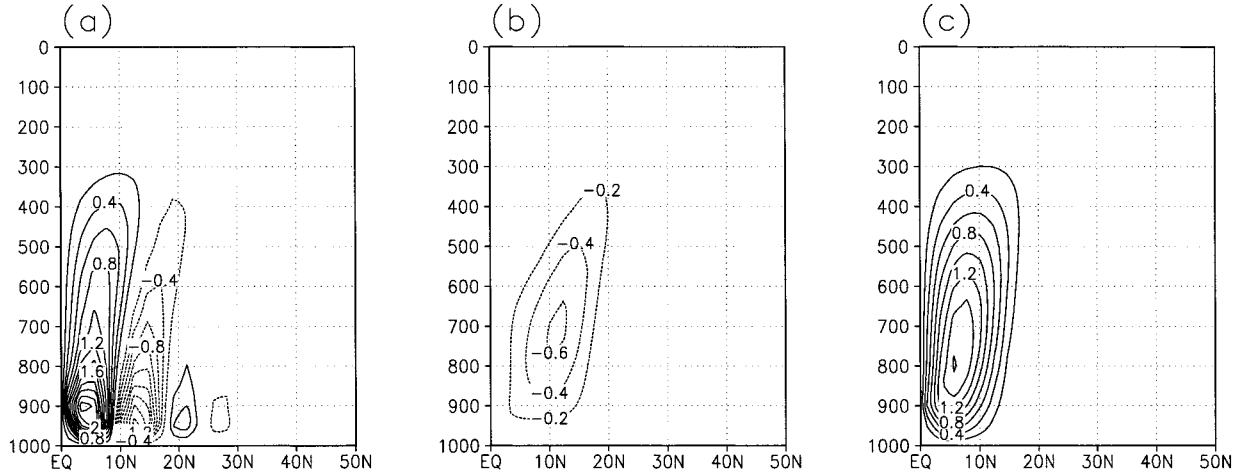


FIG. 6. Differences of QG diagnostic mass streamfunction responses between $\Theta_0\Delta_v = 5$ K and control case. (a) Approximated total difference, $\delta\Psi$; due to (b) the change in the diabatic heating (δH), and (c) the change in the static stability (δL). Contour interval is 1×10^9 kg s $^{-1}$ and zero contours are omitted.

tion, that is, (12), with all terms on the rhs of (12) included except for the first term, and $\omega^* = \omega_{\text{ctl}} + \delta\omega^*$. The sum of these two terms is displayed in Fig. 7c. This quantity compares reasonably well with δQ (see Fig. 7d), obtained from the PE model calculations, indicating that to the lowest order, (13) can be rewritten as

$$-\delta\Gamma \frac{\partial\omega^*}{\partial y} - \Gamma \frac{\partial\delta\omega^*}{\partial y} \approx \frac{\partial\delta Q}{\partial y}. \quad (14)$$

In other words, to the lowest order the contribution by $\delta\omega^H$ is negligible. Therefore, one might be tempted to make a causal statement that the change in Hadley cell strength ($\delta\omega^*$), combined with $\delta\Gamma$, leads to the nonzero δH and hence is responsible for the narrowing of the Hadley cell.

If the above causal relationship indeed exists, then as the static stability is decreased over time, the strengthening of the Hadley cell must *lead* the narrowing of the Hadley cell. In order to test this idea, we analyze the transient evolution of the MMC. Taking the steady state solution of the control case as an initial state, decrease the value of $\Theta_0\Delta_v$ from 12.5 to 5 K, and then integrate the PE model forward in time. We measure the rate at which the Hadley cell intensifies by calculating an ‘‘amplification rate,’’ \mathcal{A} , defined as

$$\mathcal{A} \equiv \frac{1}{\Delta\Psi_{\text{max}}(t)} \frac{\partial\Delta\Psi_{\text{max}}(t)}{\partial t},$$

where $\Delta\Psi_{\text{max}}(t)$ is the maximum value of the vertically averaged $\Psi(t) - \Psi_{\text{ctl}}$ at time t , with Ψ_{ctl} being the steady state streamfunction of the control case. The rate at which the Hadley cell shrinks is measured by calculating a ‘‘narrowing rate,’’ \mathcal{N} , defined as

$$\mathcal{N} \equiv -\frac{1}{\Delta\phi_{\text{min}}(t)} \frac{\partial\Delta\phi_{\text{min}}(t)}{\partial t},$$

where $\Delta\phi_{\text{min}}(t)$ is the latitude where vertically averaged $\Psi(t) - \Psi_{\text{ctl}}$ attains its largest *negative* value; narrowing of the Hadley cell results in an *anomalous* reversed cell. Thus, $\Delta\phi_{\text{min}}(t)$ represents the latitude where the anomalous reversed cell attains its peak amplitude.

Figure 8 shows the time evolution of these two rates. For display purpose, both rates are normalized by their corresponding maximum values. Consistent with the hypothesis that the narrowing of the Hadley cell is a response to the intensification, it can be seen that the maximum amplification rate *leads* the maximum narrowing rate. Furthermore, the narrowing rate approaches zero far more slowly than does the amplification rate.

6. Discussion and concluding remarks

Our least inviscid axisymmetric circulation with the multilevel PE model yields results consistent with the theory of HH. Such agreements lend confidence to our calculations and to conclusions drawn from the inter-comparisons between the axisymmetric and nonaxisymmetric MMCs, to be described in Part II of this study. On the other hand, as the Boussinesq approximation and rigid upper boundary condition are invoked in the theory of HH, one could view our analysis as a test for the validity of these idealizations.

The key advantage of the methodology adopted in this study is its capability of distinguishing between direct and indirect responses of the MMC to individual source terms. The strengthening and broadening of the Hadley cell, which is the response to an increase in the model’s viscosity, are also found to be attributable to indirect effects of the increased viscosity, that is, changes in the diabatic heating and surface friction. Likewise, when the meridional temperature gradient of the model is increased, viscosity accentuates the effect of this dia-

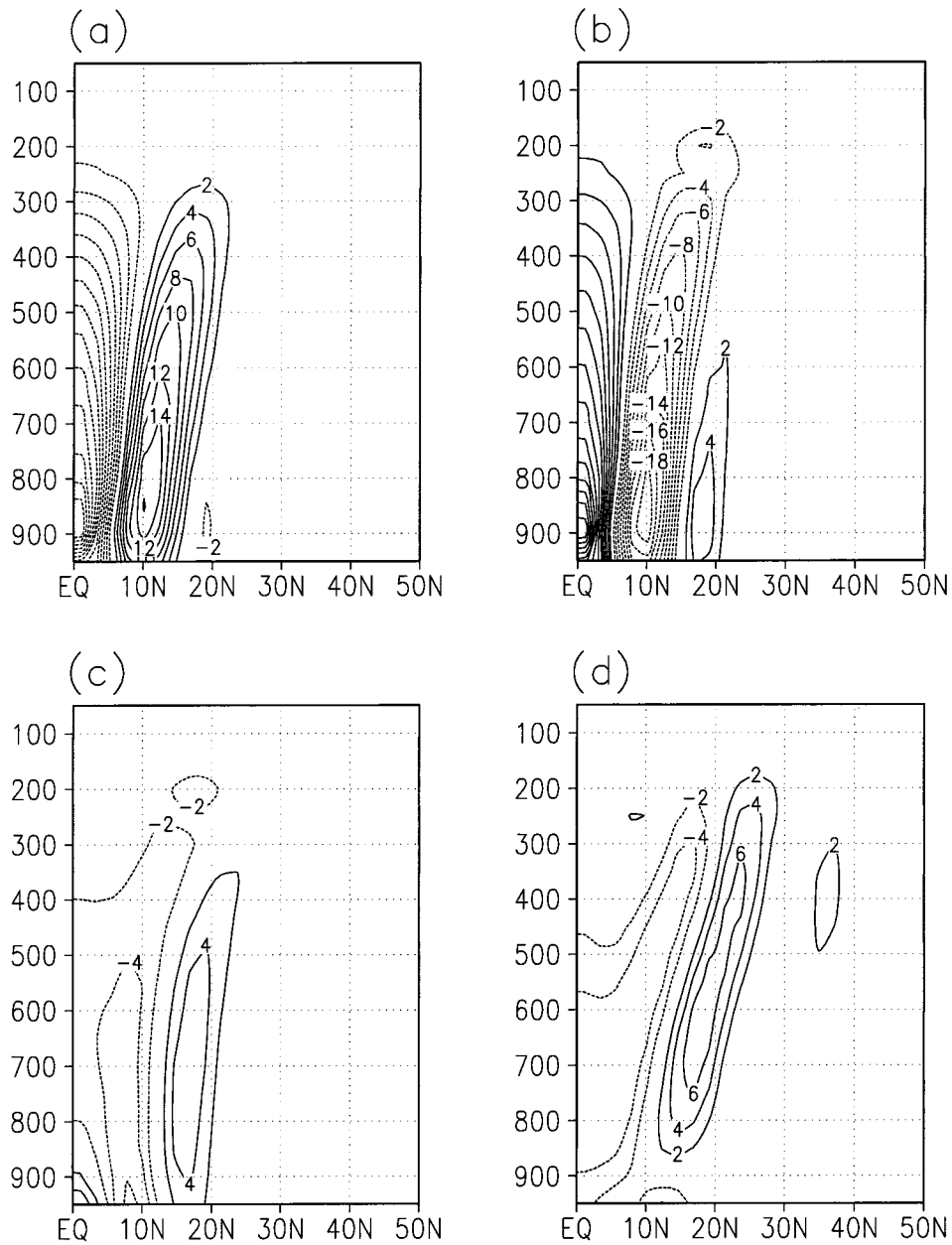


FIG. 7. (a) The change in the static stability, $-\delta\Gamma\omega^*$; (b) the change in the vertical velocity, $-\Gamma\delta\omega^*$, due to the decrease of the static stability (from $\Theta_0\Delta_p = 12.5$ to 5 K); (c) the approximate difference of the thermal forcing ($\approx -\delta\Gamma\omega^* - \Gamma\delta\omega^*$); and (d) the actual difference of the thermal forcing, δQ , obtained from the PE models. Contour interval is 2×10^{-3} K day $^{-1}$. Zero contours are omitted and dotted lines indicate negative values.

batic heating change by broadening and strengthening of the Hadley cell.

The above mechanism that couples viscosity with diabatic heating might also be relevant for the formation of the intertropical convergence zone (ITCZ). Suppose that the latitudinal distribution of tropical convection is more or less uniform throughout the tropical atmosphere. If viscosity in the tropical atmosphere represents vertical mixing of horizontal momentum by “cumulus

friction”³ (Schneider and Lindzen 1977), throughout the Tropics, convection will mix zonal momentum vertically, driving a direct cell. This direct cell will adia-

³ As summarized by Moncrieff (1997), the direction of the vertical flux of horizontal momentum by convection is very sensitive, and can be either downgradient or upgradient. Furthermore, their collective impact on the global-scale circulation is yet to be established. Our argument should be taken with this caveat in mind.

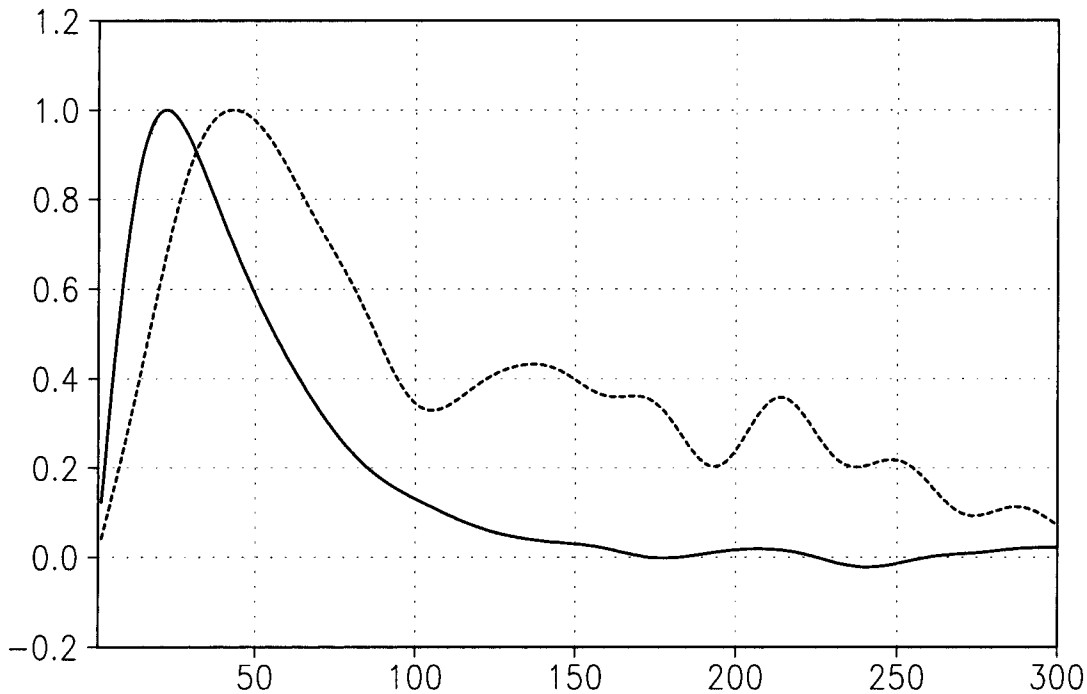


FIG. 8. Amplification rate \mathcal{A} (solid line) and narrowing rate \mathcal{N} (dotted line).

batically cool the deep Tropics, with warming elsewhere. Suppose further that this adiabatic cooling (heating) is balanced by diabatic heating (cooling). If this “viscosity-driven,” or “cumulus friction-driven” diabatic heating is realized by changes in latent heating through the changes in convection, there must be more numerous and/or vigorous convection in the deep Tropics, and less convection outside of the region. If this picture is correct, convective activity will gradually concentrate toward an increasingly narrow region in the deep Tropics. Although highly speculative at this point, the simplicity of this picture makes it an attractive mechanism for the ITCZ formation. This mechanism, if it indeed operates, may be viewed as supplementary to those described by others (e.g., Dodd and James 1997; Raymond 2000) who attribute the ITCZ formation to tropical convective heating.

For a sufficiently large variation in static stability, the Hadley cell width exhibits sensitivity to the static stability. It is found that while the Hadley cell strengthens as a direct consequence of the reduced static stability [the last term on the rhs of (12)], the narrowing of the Hadley cell is due to the change in diabatic heating [the first term on the rhs of (12)]. An additional calculation shows that the amplification of the Hadley cell leads the narrowing of the Hadley cell by about 20 days. The implication is that if the static stability fluctuates with a timescale less than this value, one might observe corresponding fluctuations in the amplitude, but not in the width, of the Hadley cell.

Acknowledgments. Comments and suggestions by Dr. Steven Feldstein on an earlier version of this manuscript are greatly appreciated. Comments by Dr. Volkmar Wirth and an anonymous reviewer, as well as suggestions made by Dr. Geoffrey Vallis, in the capacity of *Journal of the Atmospheric Sciences* editor, also improved this manuscript. This research was supported by the National Science Foundation through Grant ATM-9525977 and by the National Oceanic and Atmospheric Administration through Award NA86GP0260.

APPENDIX

Hough Functions $\Theta_n(\mu)$ and the Associated Functions $B_n(\mu)$

The Hough functions $\Theta_n(\mu)$, the associated functions $B_n(\mu)$, and the corresponding eigenvalues ϵ_n were calculated by the method described in Plumb (1982) and Haynes and Shepherd (1989). Because of the boundary condition of $B_n(\pm 1) = 0$, it is more convenient to solve the eigenvalue problem for $B_n(\mu)$ than $\Theta_n(\mu)$:

$$\frac{(1 - \mu^2)^{1/2}}{\mu^2} \frac{d^2}{d\mu^2} [B_n(\mu)(1 - \mu^2)^{1/2}] - \epsilon_n B_n(\mu) = 0. \quad (\text{A1})$$

Upon solving for $B_n(\mu)$, $\Theta_n(\mu)$ is calculated using (9). However, for sufficiently large n , inaccuracies in the structure of $\Theta_n(\mu)$ arise when one tries a straightforward centered finite differencing. As shown in Fig. A1a, this leads to a violation of orthogonality at large n . If $\Theta_n(\mu)$ are orthogonal to each other, the diagonal elements of

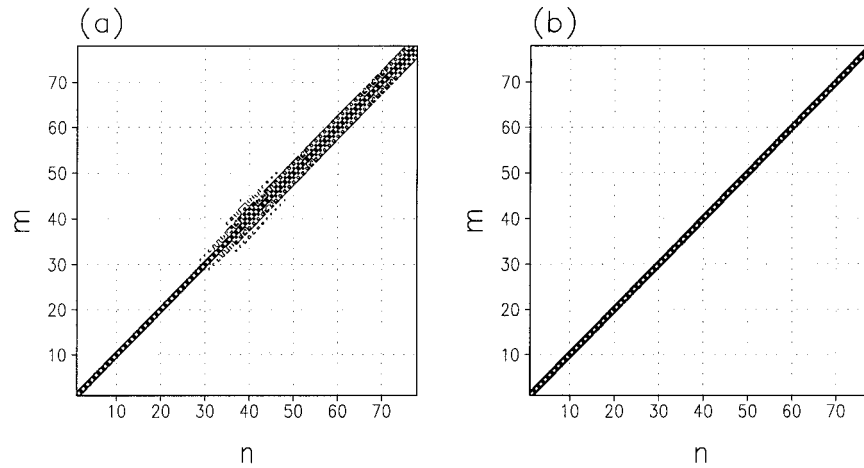


FIG. A1. Orthogonality condition of Hough function $\Theta_n(\mu)$ obtained by using (a) original $B_n(\mu)$ and (b) interpolated $B_n(\mu)$ (δ_{nm}).

diagram should be one, and elsewhere they must be zero [see (A3)]. Up to mode $n = 28$, the $\Theta_n(\mu)$ are orthogonal to each other, however orthogonality is lost for higher value of n because of the inaccuracies involved in the finite differencing of $B_n(\mu)$, whose scale becomes increasingly small (infer the trend from Figs. A3c,d). We

found that impact of this inaccuracy is minimal for the extratropical circulations, however, it can greatly distort the forcing and response in the Tropics. For example, consider the thermal forcing, Q , and its response for the control axisymmetric flow. One finds that the Q (Fig. A2c), reconstructed from $Q_n(p)$, given by

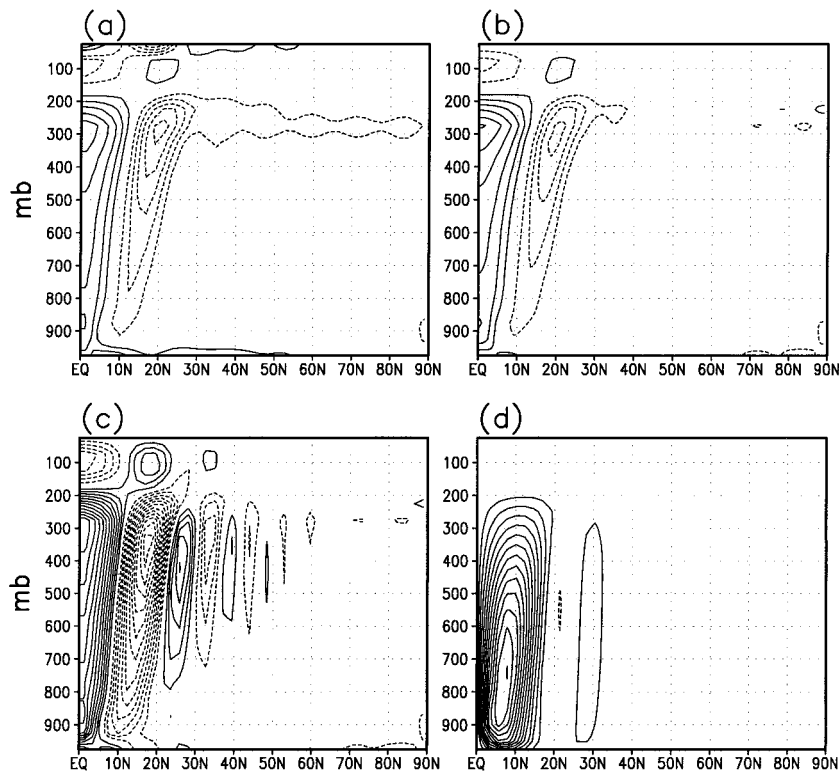


FIG. A2. Thermal forcing $Q(\mu, p)$ (a) in the control axisymmetric flow; (b) recalculated from $Q_n(p)$, which is obtained by using interpolated $B_n(\mu)$, and (c) recalculated from $Q_n(p)$ using original $B_n(\mu)$ through transformations. (d) QG mass streamfunction using (c) as a thermal forcing. Contour interval in (a), (b), and (c) is $1 \times 10^{-7} \text{ K s}^{-1}$ and in (d) $1 \times 10^9 \text{ kg s}^{-1}$. Zero contours are omitted and dotted lines indicate negative values.

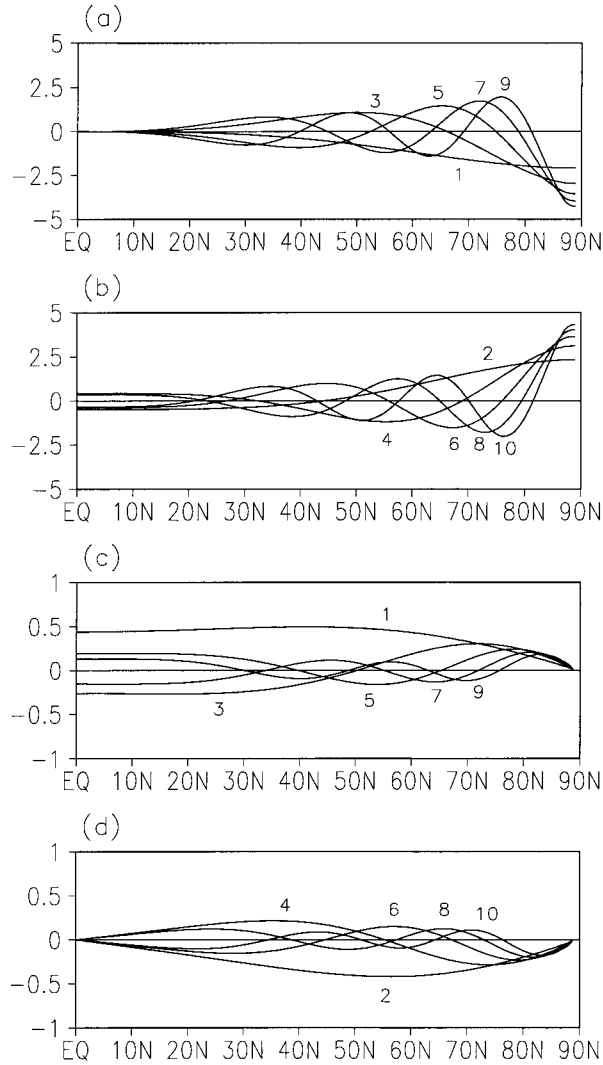


FIG. A3. Structure in $0 \leq \theta \leq 90^\circ\text{N}$ ($0 \leq \mu \leq 1$) of the first 10 Hough functions $\Theta_n(\mu)$ and the associated functions $B_n(\mu)$: (a) Θ_n odd modes, (b) Θ_n even modes, (c) B_n odd modes, and (d) B_n even modes.

$$Q_n(p) = \int_{-1}^1 Q(\mu, p) \Theta_n(\mu) d\mu, \quad (\text{A2})$$

is much stronger than the actual Q (Fig. A2a). This results in a much too strong Ψ response (Fig. A2d; compare with Fig. 2). Calculation of $\Theta_n(\mu)$ in the spectral domain does not remedy this problem, because the structure of $B_n(\mu)$ is different from Legendre polynomials, again introducing inaccuracies. Also, it should be noted that resolution increase, for example, using R60 rather than R30, does not solve the problem either. This is because the increased resolution will introduce even higher order modes. Again for sufficiently large n , the meridional resolution will not be high enough to yield accurate finite differencing.

There are various ways to resolve the inaccuracy problem. We chose to calculate $B_n(\mu)$ using double pre-

TABLE A1. The Hough mode eigenvalues ϵ_n .

n	ϵ_n	Longuet-Higgins
1	-8.156	-8.127
2	-12.595	-12.543
3	-35.613	-35.420
4	-44.980	-44.732
5	-82.817	-82.384
6	-97.086	-96.618
7	-149.510	-149.061
8	-168.570	-168.225
9	-235.140	-235
10	-258.830	-260

cision followed by a transformation into higher resolution using a cubic spline interpolation method (Press et al. 1992). We found 317 meridional grid points are sufficient to obtain an orthogonal $\Theta_n(\mu)$ (cf. there are 80 meridional grid points for R30 truncation). Figure A1b shows that when the interpolated $B_n(\mu)$ is used, the $\Theta_n(\mu)$ are orthogonal to each other for all values of n . With an improved $\Theta_n(\mu)$, a much more precise MMC is obtained. Figure A2b shows the recalculated Q from $Q_n(p)$ using the new $\Theta_n(\mu)$, which is much closer to the true Q (Fig. A2a). The overall structure of the diagnosed Ψ (Fig. 2) becomes similar to that of the PE model (Fig. 1a) although the former is somewhat weaker than the latter.

Because the inaccuracy in the finite differencing manifests itself in the forcing and responses in low latitudes, without an appropriate correction as described above, a discrepancy between the diagnosed Ψ and that from the PE model can easily be attributed to the shortcomings of the QG approximation in the Tropics. As will be shown in KL, except when very strong diabatic heating is imposed, the performance of the MMC equation is surprisingly reliable even in the Tropics.

In order to complete the description of the Hough function, in Table A1, we list the Hough mode eigenvalues, ϵ_n . These values are much closer to those of Longuet-Higgins (1968, Table 10 therein) than those given by Plumb (1982). Consistently, the structure of $\Theta_n(\mu)$ and $B_n(\mu)$ (see Fig. A3) are slightly different from those of Plumb (see Fig. 1 in that paper). The first 10 leading modes of $\Theta_n(\mu)$ and $B_n(\mu)$, shown in Fig. A3, are normalized to satisfy the following equations:

$$\int_{-1}^1 \Theta_n(\mu) \Theta_m(\mu) d\mu = \delta_{nm}, \quad \text{and} \quad (\text{A3})$$

$$-\epsilon_n \int_{-1}^1 \mu^2 B_n(\mu) B_m(\mu) d\mu = \delta_{nm}. \quad (\text{A4})$$

REFERENCES

- Becker, E., G. Schmitz, and R. Geprags, 1997: The feedback of mid-latitude waves onto the Hadley cell in a simple general circulation model. *Tellus*, **49A**, 182–199.

- Chang, E. K. M., 1996: Mean meridional circulation driven by eddy forcings of different timescales. *J. Atmos. Sci.*, **53**, 113–125.
- Dodd, J. P., and I. N. James, 1997: The impact of latent-heat release on the Hadley circulation. *Quart. J. Roy. Meteor. Soc.*, **123**, 1763–1770.
- Eliassen, A., 1951: Slow thermally or frictionally controlled meridional circulation in a circular vortex. *Astrophys. Norv.*, **5**, 19–60.
- Feldstein, S. B., 1994: A weakly nonlinear primitive equation baroclinic life cycle. *J. Atmos. Sci.*, **51**, 23–34.
- Haynes, P. H., and T. G. Shepherd, 1989: The importance of surface pressure changes in the response of the atmosphere to zonally-symmetric thermal and mechanical forcing. *Quart. J. Roy. Meteor. Soc.*, **115**, 1181–1208.
- Held, I. M., and A. Y. Hou, 1980: Nonlinear axially symmetric circulations in a nearly inviscid atmosphere. *J. Atmos. Sci.*, **37**, 515–533.
- Kim, H., and S. Lee, 2001: Hadley cell dynamics in a primitive equation model. Part II: Nonaxisymmetric flow. *J. Atmos. Sci.*, **58**, 2859–2871.
- Kuo, H.-L., 1956: Forced and free meridional circulations in the atmosphere. *J. Meteor.*, **13**, 561–568.
- Lindzen, R. S., and B. Farrell, 1980: A simple approximate result for the maximum growth rate of baroclinic instabilities. *J. Atmos. Sci.*, **37**, 1648–1654.
- Longuet-Higgins, M. S., 1968: The eigenfunctions of Laplace's tidal equations over a sphere. *Philos. Trans. Roy. Soc. London*, **262A**, 511–607.
- Moncrieff, M. W., 1997: Momentum transport by organized convection. *The Physics and Parameterization of Moist Atmospheric Convection*, R. K. Smith, Ed., NATO ASI Series, Series C, Vol. 505, Kluwer Academic, 231–253.
- Pfeffer, R. L., 1981: Wave-mean flow interactions in the atmosphere. *J. Atmos. Sci.*, **38**, 1340–1359.
- Plumb, R. A., 1982: Zonally symmetric Hough modes and meridional circulations in the middle atmosphere. *J. Atmos. Sci.*, **39**, 983–991.
- , and J. Eluszkiewicz, 1999: The Brewer–Dobson circulation: Dynamics of the tropical upwelling. *J. Atmos. Sci.*, **56**, 868–890.
- Press, W. H., S. A. Teukolsky, W. T. Vetterling, and B. P. Flannery, 1992: *Numerical Recipes in Fortran 77*. 2d ed. Cambridge University Press, 933 pp.
- Raymond, D. J., 2000: The Hadley circulation as a radiative-convective instability. *J. Atmos. Sci.*, **57**, 1286–1297.
- Schneider, E. K., 1977: Axially symmetric steady-state models of the basic state for instability and climate studies: Part II. Nonlinear calculations. *J. Atmos. Sci.*, **34**, 280–297.
- , and R. S. Lindzen, 1977: Axially symmetric steady-state models of the basic state for instability and climate studies: Part I. Linearized calculations. *J. Atmos. Sci.*, **34**, 263–279.